Steel and Composite Structures, *Vol. 33, No. 1* (*2019*) *1-18*
DOI: https://doi.org/10.12989/scs.2019.33.1.001

Seismic performance of steel plate shear walls with variable column flexural stiffness

Ivan Curkovic*, Davor Skejic [a] and Ivica Dzeba [b]

Department of Structures, *University of Zagreb*, *Faculty of Civil Engineering*, *Kaciceva 26*, *10000 Zagreb*, *Republic of Croatia*

(*Received November 14, 2018, Revised March 6, 2019, Accepted September 26, 2019*)

Abstract. In the present study, the behavior of steel plate shear walls (SPSW) with variable column flexural stiffness is experimentally and numerically investigated. Altogether six one-bay one-story specimens, three moment resisting frames (MRFs) and three SPSWs, were designed, fabricated and tested. Column flexural stiffness of the first specimen pair (one MRF and one SPSW) corresponded to the value required by the design codes, while for the second and third pair it was reduced by 18% and 36%, respectively. The quasi-static cyclic test result indicate that SPSW with reduced column flexural stiffness have satisfactory performance up to 4% story drift ratio, allow development of the tension field over the entire infill panel, and cause negligible column "pull-in" deformation which indicates that prescribed minimal column flexural stiffness value, according to AISC 341-10, might be conservative. In addition, finite element (FE) pushover simulations using shell elements were developed. Such FE models can predict SPSW cyclic behavior reasonably well and can be used to conduct numerical parametric analyses. It should be mentioned that these FE models were not able to reproduce column "pull-in" deformation indicating the need for further development of FE simulations with cyclic load introduction which will be part of another paper.

Keywords: steel plate shear wall; tension field theory; quasi-static cyclic testing; column flexural stiffness; finite element model

1. Introduction

In past few decades steel plate shear walls (SPSWs) have seen increased use as vertical stabilization systems, i.e., lateral load resisting systems, particularly in buildings which require ductile seismic behaviour. Since Eurocodes, up to date, still do not recognize them they have been mostly implemented in the USA, Canada and Japan, (Astaneh-Asl 2001, Sabelli and Bruneau 2007). Typically SPSWs, as the one in Fig. 1, consist of thin unstiffened steel infill plate connected to columns (vertical boundary elements (VBEs)) on each side, and beams (horizontal boundary elements (HBEs)) above and below. These infill plates are allowed to buckle under shear load and subsequently form diagonal tension fields when resisting lateral loads. Also, to additionally increase buckling strength of the infill plates various infill plate types (Kalali *et al*. 2015), as well as stiffener arrangements on the infill plate have been investigated in the past (Rahmzadeh *et al*. 2016). SPSWs exhibit high stiffness and strength, behave in a ductile manner, and are able to dissipate large amounts of hysteretic energy, which make them viable option for the design of new buildings as well as for the retrofit of the existing structures (Sabelli and Bruneau 2007).

Design of SPSWs is based on the capacity design approach where yielding of the material is expected to occur within the infill plate, while HBEs and VBEs are to be designed to remain elastic. The only exception is that, for development of the expected load bearing mechanism, plastic hinges at HBEs ends and VBEs bases are allowed to form when using rigid beam-to-column and column base joints, respectively. Another important fact when designing SPSWs is the assumption that the entire lateral load is carried by the steel infill panel alone while the contribution of the moment resisting frame (MRF) to the total strength should not be taken into account. Therefore, nominal strength of the SPSW system, V_n, is calculated as the strength of infill plate alone when the tension field forms using following expression from AISC 341 (AISC 2010)

$$V_n = 0.42 t_w L_{cf} f_y \sin 2\alpha \quad (1)$$

where t_w is the infill panel thickness, L_{cf} is the clear distance between column flanges, f_y is the infill panel yield strength, and α is angle between infill panel tension diagonals and column axis in degrees calculated per expression (F5-2) in AISC 341 (2010). The Eq. (1) is derived from Basler's expression for the shear strength of steel plate girders in (Basler 1961) omitting the first part corresponding to the plate critical shear force and reducing plate post-critical strength by 20% according to Berman and Bruneau (2003). Plate critical shear force is omitted due fact that panels of SPSW are very slender plates which lose their stability almost immediately after load application. Fig. 1 presents stress distribution in SPSWs assuming formation of the

*Corresponding author, Ph.D.,
E-mail: icurkovic@grad.hr
[a] Associate Professor
[b] Professor

ISSN: 1229-9367 (Print), 1598-6233 (Online)

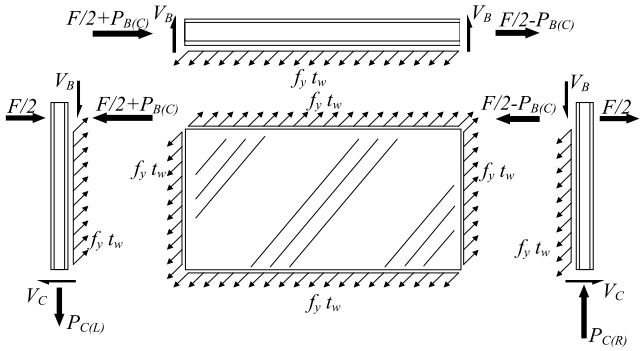

Fig. 1 Stress distribution to boundary elements in SPSW assuming formation of the tension field (Sabelli and Bruneau 2007)

tension field within the infill panel, where F is the applied lateral load, $P_{B(C)}$ is the axial force applied at the end of the beam due to tension field action on the column, $P_{C(L/R)}$ is the axial force reaction in left or right column, and V_B and V_C are the shear reactions of the beam and column due to tension field action, respectively.

In order for the tension field to develop over the entire infill plate and to achieve presented stress distribution, HBEs and VBEs need to have adequate strength and stiffness. Strength and stiffness requirements are usually easily satisfied for intermediate HBEs where tension field action from upper and lower plate mostly cancel each other out if the thickness of the adjacent infill plates is the same. However, the problem is pronounced within the columns (VBEs) as well as top and bottom (foundation) HBEs, since these elements are exposed only to one-sided tension field action. For that purpose numerous simplified analytical models for design and analysis of SPSWs systems have been proposed and validated (Berman and Bruneau 2003, Thorburn *et al.* 1983, Elgaaly *et al.* 1993, Driver *et al.* 1998, Purba and Bruneau 2010, Qin *et al.* 2017a, b). Additionally, after the test results of quarter-scale SPSW specimens provided in (Lubell *et al.* 2000), where VBE exhibited significant "pull-in", strength-based design approach was complemented with boundary elements (HBEs and VBEs) stiffness requirement based on observations made by Montgomery and Medhekar (2001) as described in following chapter.

Qu and Bruneau (2010) have already, using analytical methods, considered issue regarding column flexural stiffness requirement. Their results showed no correlation between column flexural stiffness and significant "pull-in" deformations of. In spite of these results, Qu and Bruneau noticed that, in the future, additional experimental and analytical research should be conducted in order to investigate if other concerns might exist that may justify the application of column flexural stiffness. Aditionally, Machaly *et al.* 2014, also concluded that when either number of floors or the infill panel tensile strength increases flexural, as well as axial rigidity of columns needs to be increased in order to achieve full plastic mechanism within the steel plate. Therefore, in order to further investigate the requirement regarding VBEs flexural stiffness, this research was conducted. Here, unlike in the available literature, capacity design approach was used in order to obtain required strength of boundary elements, which allows clear examination of only column flexural stiffness influence on the SPSW behaviour. The research was divided into two parts - experimental and numerical. During the experimental investigation tests were conducted on MRFs without infill and SPSW specimens with variable column flexural stiffness. Detailed experimental results were afterwards used to calibrate numerical pushover model.

2. Column flexural stiffness requirement

Steel infill plates, due to their thickness, present very slender elements having low value of critical buckling shear force which results in early formation of tension diagonals and eventually, if the boundary conditions are adequate, formation of the tension field over the entire plate. Wagner (1931) was first to introduce flexibility factor, ω_h, as an index of plate girder flange flexibility, which is related to the ability of uniform stress development within the tension field. Since SPSWs can be considered as plate girders, where plate girder flanges present VBEs, flexibility factor of column, using few assumptions, can thus analogously be expressed as (Montgomery and Medhekar 2001)

$$\omega_h \approx 0.7H\sqrt[4]{\frac{t_w}{2I_cL}} \tag{2}$$

where H presents the storey height, t_w is the infill panel thickness, I_c is second moment of area of each column and L is the SPSW width. In order to determine minimum flexural stiffness value of VBEs needed to ensure uniform formation of the tension field in SPSWs, the value of the flexibility factor was limited to value of 2.5 (CSA 2009). Limiting the value of flexibility factor to 2.5 corresponds to state where maximum stress within the tension field does not exceed the average stress by more than 20% (Kuhn *et al.* 1952). Therefore, imposing the upper bound of 2.5 in Eq. (2) and solving for I_c results with the lowest allowable column flexural stiffness that is currently used (AISC 2010, CSA 2009)

$$I_c \geq \frac{0.0031t_wH^4}{L}. \tag{3}$$

To evaluate suitability of code compliant column flexibility factor, i.e., application of column flexural stiffness requirement, experimental and numerical investigations were conducted (Curkovic *et al.* 2017). Furthermore, due to lack of research on composite plate shear walls (CPSWs) (Curkovic and Dzeba 2016), the requirement in Eq. (3) is also used for their design (AISC 2010) even though such vertical stabilization systems have more favorable stress distribution from the infill panel to the boundary elements than is the case in SPSWs. The results investigating behavior of SPSWs are presented here, while the ones investigating behaviour of CPSWs will be presented in accompanying paper.

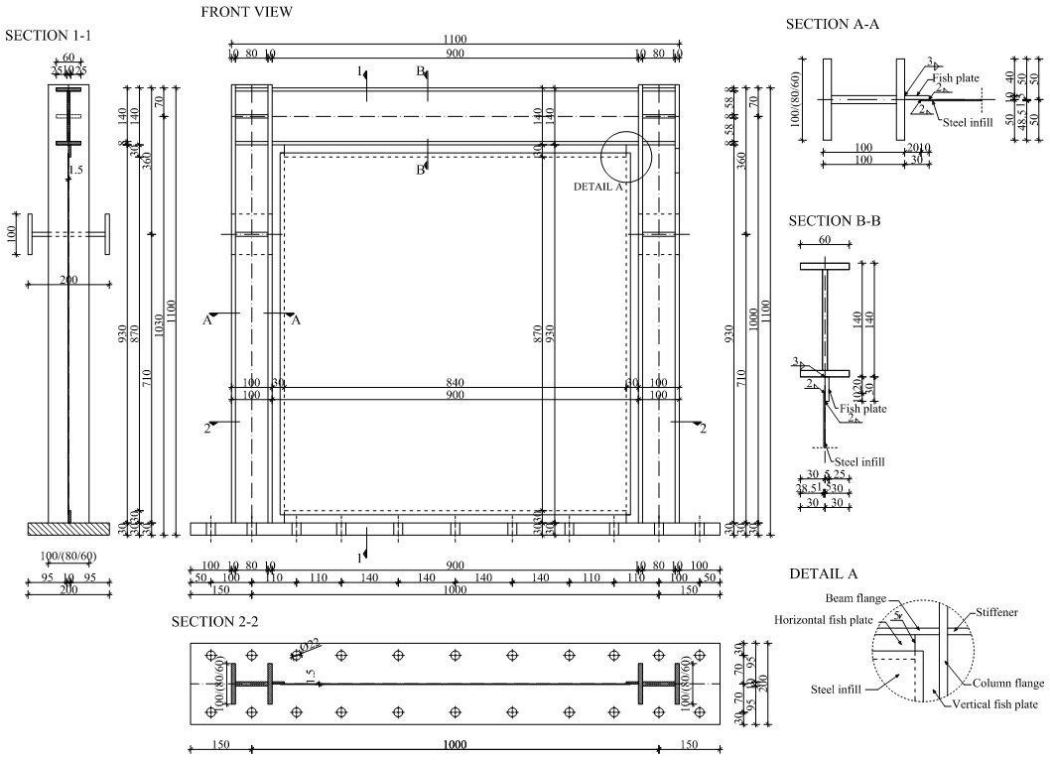

Fig. 2 SPSW specimen geometry and details (units are in mm)

3. Experimental programme

3.1 General

The experimental research was conducted at the Faculty of Civil Engineering at the University of Zagreb, Croatia within the framework of the Ph.D. dissertation (Curkovic 2017). Specimens were divided in specimen groups F and S within which MRF and SPSW specimens were tested, respectively. In order to study the influence of column flexural stiffness on the seismic behaviour of SPSWs, three scaled specimens with varying column flexibility were tested. Additionally, in order to determine the contribution of the steel frame alone to the stiffness and load bearing capacity of the SPSWs, three analogue MRFs specimens, with same column flexural stiffness as SPSW specimens, were tested.

3.2 Preparation of the specimens

For the experimental investigations, three one-story one-bay specimens within each specimen group (F and S) with scale of 1:4 were designed and fabricated. Height of the scaled specimens was 1030 mm and the bay span was 1000 mm, Fig. 2. Three specimens with modified column geometry were tested within each of the two specimen groups.

Design of the specimens was conducted in accordance with EN 1993-1-1 (CEN 2005), taking into account general rules provided for seismic design of steel buildings in EN 1998-1 (CEN 2004). As EN 1998-1 (CEN 2004) does not provide any guidelines for SPSWs design, their design was carried out according to requirements of AISC 341 (2010) and CSA S16 (2009). Also, due to scarcity of the guidelines provided in those design codes, and in order to avoid unwanted failure mechanisms that were recorded in previous research, (Lubell *et al.* 2000, Qu and Bruneau 2010), strength design criteria proposed in other available literature, (Qu and Bruneau 2010, Vian 2005, Park *et al.* 2007, Tsai *et al.* 2014), were additionally used.

Due to actuator load limitation of 600 kN, the assumption that the infill steel plate resists entire lateral load and in order to conduct experiment up to a failure point 1.5 mm thick infill steel plate was chosen for the SPSW specimens. Afterwards, boundary elements were designed using capacity design approach. Boundary elements cross-sections of the reference specimen (specimens with label 100) were chosen in order to satisfy smallest allowed value of column second area moment, I_c, adopted in AISC 341 (2010), and CSA 16 (2009), for SPSWs. Column flexural stiffness variation of the remaining specimens was achieved through reduction of column flanges width, which has been done in 20 mm increments. Therefore, an overall column flanges width reduction of 20 mm (specimens with label 80) and 40 mm (specimens with label 60) resulted with column second area moment values that were 82% and 64% of the column second area moment value used with the reference specimen, respectively. This approach was accepted in order to avoid reduction of column shear area, therefore preventing column failure in shear, which could otherwise result in premature failure of the entire system, (Qu and Bruneau 2010). Compared to reference specimen, reduction of column flanges width by 20 mm and 40 mm reduced column flexural strength by 17% and 34%, respectively.

Design of the beam was conducted for the most unfavourable situation and its cross-section has not been changed during the testing. The described approach resulted in use of built-up I shaped sections in order to satisfy all the necessary design and experimental requirements.

Application of compression force to the specimen columns was omitted due to fact that this would require greater column flexural strength which would in turn increase flexural stiffness of the columns. The obtained column geometry would easily satisfy the proposed flexural stiffness requirement, given in Eq. (3), making it impossible to analyse influence of minimum column flexural stiffness requirement on SPSW behaviour, which is the main goal of this work.

Rigid beam-to-column joints were used. Connection between the infill plate and the boundary elements was over the fish plates and was continuous over the entire infill plate and fish plate perimeter. In order to minimize initial imperfections and possible residual stresses within the infill plate special attention was given to its welding procedure. Namely, welding was conducted using MAG process where welds were carried out in several stages. Fig. 3 shows the welding sequence used. Fish plates with dimension of 30 × 5 mm were welded to the surrounding elements using fillet welds. Since specimens did not have foundation beam columns as well as bottom fish plate were welded directly to 30 mm thick base plate, which was then further bolted to the reaction frame. The use of foundation beam was omitted due to the laboratory set-up in order to obtain specimens with approximately 1:1 width-to-aspect ratio. Base plate and reaction frame were connected using M20 10.9 bolts with pretension which simulated realistic situation, i.e.,fixed column base at the building bottom storey. Also, as foundation beam flexural stiffness is usually high, omitting the foundation beam in the experiment would not influence the results, particularly here where the values of column flexural stiffness, which are being investigated, are much lower than the ones of the foundation beam itself. Fig. 2 shows final SPSWs geometry with details, while geometry of the MRF specimens is identical but without the infill and fish plates.

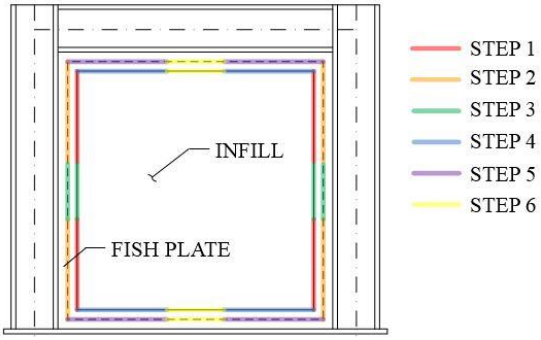

Fig. 3 Schematic view of the infill to fish plate welding sequence

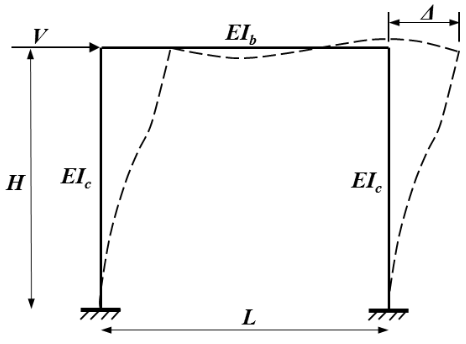

Fig. 4 Flexural deflection of frame due to lateral load

After definition of the specimen geometry it is possible to calculate specimen's initial stiffness using known analytical methods. Lateral load on top of the MRF would cause flexural deflection where column bases can be considered as fixed, while the rotation at the top of the column should be considered, Fig. 4. Initial stiffness of the MRF is therefore calculated using Eq. (4)

$$k = \frac{24EI_c}{H^3}\frac{12\rho + 1}{12\rho + 4}. \quad (4)$$

where ρ = [(EI_b)/L]/[(2EI_c)/(H)], and I_b is second moment of area of the beam.

On the other hand, initial stiffness of SPSW would be dependent on the stiffness of the frame and the plate. If the plate is assumed as fix-ended cantilevered wall its stiffness due to shear effect can be computed using equation (Timoshenko and Young 1968)

$$k = \frac{lt_w G}{1.2h}. \quad (5)$$

where l and h are length and height of the infill plate, respectively, G is wall shear modulus and V is the lateral load acting on top of the plate. Shear stiffness of the steel frame which is part of the SPSW can be calculated as per Sabouri-Ghomi and Sajjadi (2012) assuming formation of plastic hinges at the column top and bottom, which turned out to be the case in our experiments In that case MRF shear stiffness can be calculated using Eq. (4) under the assumption that $EI_b = \infty$. Finally, SPSW initial stiffness is calculated through summation of shear stiffness of the infill plate and frame. Theoretically obtained initial stiffness values of tested specimens, using experimentally obtained material data in section 3.4, are given in Table 1. The obtained values show that initial stiffness of frame with the steel infill plate is almost one order of magnitude higher than the initial stiffness of frame alone.

Table 1 Theoretical initial stiffness values of tested specimens

Specimen	Initial stiffness [kN/mm]	Specimen	Initial stiffness [kN/mm]
F100	15.2	S100	103.9
F80	13.0	S80	100.1
F60	10.7	S60	96.2

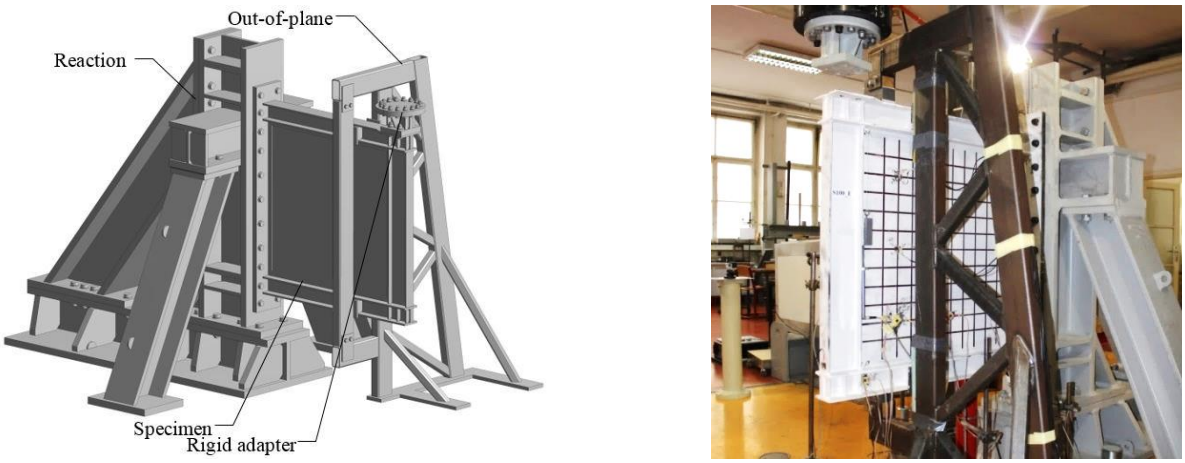

Fig. 5 Experimental test setup

3.3 Test setup and measuring devices

Due to vertical placement of the actuator the test set-up was placed in the rotated position by 90°, Fig. 5. The main components of the test set-up were supporting reaction frame, lateral bracing truss, hydraulic actuator, rigid adapter for force/displacement input and the specimens. The reaction frame and bracing lattice were bolted to the strong floor. Lateral out-of-plane displacements of the specimen were restrained by lateral bracing truss which did not provide any restriction in the in-plane direction. Due to strong floor connecting places, as well as actuator displacement, it had to be offset from the storey beam centreline to the reaction frame. Finally, it was placed at 740 mm measured from the bottom edge of the specimen, Fig. 5.

Before the experiment, gridlines were painted on top of the infill steel plates after which all specimens were whitewashed. Specimens were equipped with linear variable differential transducers (LVDT) linear strain gauges and strain gauge rosettes Figs. 6(a)-(b). The amount of measuring devices varied within each specimen group, and all the measuring places are described in Table 2. Column labelled "Spec." within Table 2 lists the specimen or specimen groups for which particular measuring device were active. To be noted is that, since the specimens were tested in the rotated position by 90°, vertically measured values represent horizontal values and vice versa.

Measuring places L1 to L4 were used to obtain column horizontal displacement profile in order to check if the "pull-in" of column occurs. Relative displacement between specimen and reaction frame at point L9 was monitored to check if the rigid connection was appropriately simulated. Measuring points L10 and L11 were used to measure horizontal and vertical displacements, respectively, that could occur due to fact that reaction frame was not absolutely immobile. Displacements at measuring point L12 were measured only for S80 and S60 in order to determine moment when the infill steel plate starts to buckle. Strain gauges were installed at critical points and probable nonlinear zones of the infill plate and boundary elements. The locations of probable nonlinear zones were based on

Table 2 Description of all available measuring places during experimental testing

Label*	Description	Spec.	Label*	Description	Spec.
L1 – L4	column horizontal displacement	F, S	**T1, T2**	column flange deformation, horizontal direction	F, S
L5, L6	steel frame diagonal length	F, S	**T3**	beam flange deformation, vertical direction	F, S
L9	rel. displ. of specimen column to reaction frame	F, S	**T4 – T7**	infill steel plate deformation, diagonal dir. 45°	S
L10	specimen bottom vertical displacement	F, S	**R1**	column web deformation, vertical direction	F, S
L11	reaction frame top horizontal in-plane displ.	F, S	**R2**	column web deformation, horizontal direction	
L12	infill steel plate out-of-plane displacement	S80, S60	**R3**	column web deformation, diagonal direction 45°	
FORCE	piston force	F, S	**R4, R7, R10**	infill plate deformation, vertical direction	S
DISPL.	piston vertical displacement	F, S	**R5, R8, R11**	infill plate deformation, horizontal direction	
			R6, R9, R12	infill plate deformation, diagonal direction 45°	

*prefix: L – LVDT, T – linear strain gauge, R – strain gauge rosette

Table 3 Mechanical properties of base structural steel material

Element	Steel designation		Proof strength at 0.2% strain	Yield strength	Ultimate strength	Modulus of elasticity	Elongation after fracture
			[MPa]	[MPa]	[MPa]	[GPa]	[%]
Plate t = 1.5 mm	DC01Am	mean	194	-	309	175.1	36.0
		S.D.	6.1	-	1.7	30.6	0.4
Plate t = 5 mm	S235JR+N	mean	281	277	415	180.0	30.1
		S.D.	13.0	-	7.3	6.2	1.6
Plate t = 6 mm	S355J2+N	mean	374	394	522	178.4	24.6
		S.D.	1.9	2.5	4.8	9.6	1.4
Plate t = 8 mm	S355J2+N	mean	341	350	481	195.8	26.6
		S.D.	5.5	6.8	4.4	19.3	0.3
Plate t = 10 mm	S355J2+N	mean	356	358	511	196.3	25.2
		S.D.	1.3	2.7	2.3	3.8	1.6

finite element analyses. Strain gauges at the infill steel plates were arranged at numerous points in order to determine if the tension field was able to develop over the entire infill.

3.4 Material properties

Hot rolled steel grade S355J2+N was used for specimen boundary elements (6, 8 and 10 mm thick plates), steel grade S235JR+N was used for fish plates (5 mm thick plate), while the 1.5 mm thick infill steel plate was made out of cold rolled steel DC01Am (EN 10130:2006). Steel plate with lower yield strength was used in order to test specimens up to failure point, but also due to reason that higher yield strength would, again, increase column flexural stiffness, therefore making column strength relevant design requirement. In order to determine steel properties monotonic tensile testing according to EN ISO 6892-1 (CEN 2009), was conducted. Total of four tensile coupons were selected from each steel plate – two in the direction of rolling and two perpendicular to it. The obtained mechanical properties of the steel materials, with corresponding mean and standard deviations values are presented in Table 3. Additional details on material testing procedure and results can be found in (Curkovic 2017).

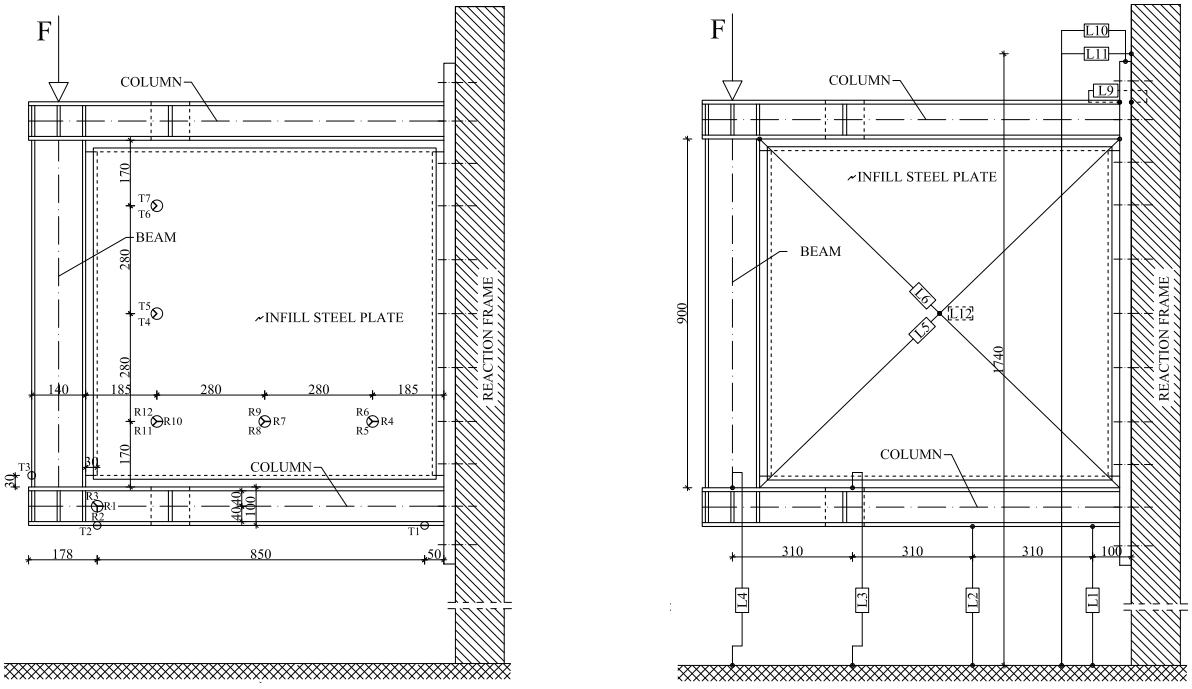

(a) Strain gauges (b) LVDT devices

Fig. 6 Position of measuring devices (units are in mm)

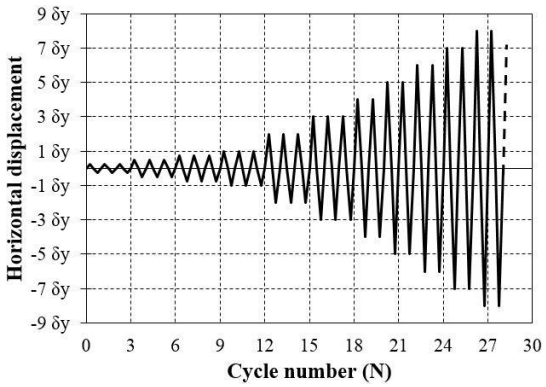

Fig. 7 Cyclic displacement loading history

3.5 Loading protocol

The loading protocol was applied through the hydraulic actuator using displacement control procedure. The specimens were loaded with quasi-static cyclic loading and the loading protocol was defined according to ECCS (1985) and ATC-24 (ATC 1992). In order to define the displacement amplitude of each load cycle within the loading protocol yield displacement, δ_y, had to be determined. Yield displacement, δ_y, was determined using numerical finite element analysis of the specimen models. Since there is no single procedure defined for numerical determination of the yield displacement, δ_y, the approach used in (Purba and Bruneau 2014) was applied. Therefore, the yield displacement, δ_y, was determined as intersection of elastic and inelastic tangents placed on the numerically obtained force-displacement (F-δ) diagram. As the initial stiffness of specimens within the two specimen groups was significantly different, two values of yield displacement were determined for each specimen group. The chosen yield displacement for specimen group F and group S was 11 mm and 3 mm, respectively.

The cyclic displacement loading history in terms of δ_y and number of cycles per each displacement amplitude are illustrated in Fig. 7. The displacement amplitudes of the loading protocol were 0.25 δ_y, 0.5 δ_y, 0.75 δ_y, and δ_y after which displacement amplitudes increased by an increment of δ_y. All test were conducted up to the specimen failure point. Loading cycles up to and including the displacement amplitude of 3 δ_y were repeated three times, after which repetitions of the loading cycles dropped to two.

Load was applied at the level of the storey beam and the transfer from the actuator to the test specimen was over the rigid steel adapter, Fig. 5. Additionally, to be noted is that, since the test set-up specimen was in the rotated position, compression (C) and tension (T) in the actuator resulted in downward and upward movement of the specimen, respectively.

4. Experimental results and discussion

4.1 General

To study the contribution of the MRFs to the stiffness and load bearing capacity of SPSWs as well as the effect of

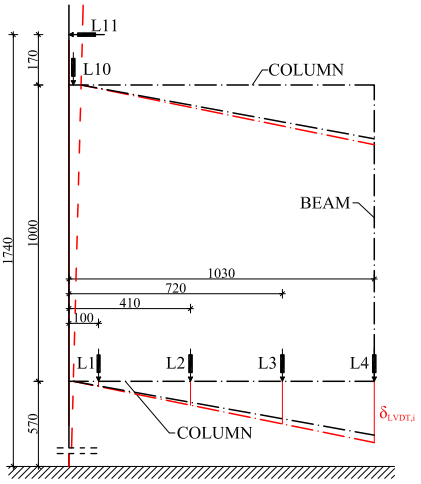

Fig. 8 Displacement correction scheme (units are in mm)

column flexural stiffness on the cyclic behaviour of SPSWs cyclic tests were conducted during experimental program. Behaviour of each specimen was carefully captured during the entire loading protocol. The comparison of specimen behaviour was conducted on multiple levels using initial stiffness values, load bearing capacity, ductility, energy dissipation capacity, damping ability, secant stiffness reduction, and column horizontal displacements profile.

As previously mentioned, although the reaction frame was much stiffer than the specimens, due to bolted connections between its elements it was not completely immobile and therefore observed small displacements. These displacements were recorded at measuring points L10 and L11 and were used to correct values recorded at L1 to L4 measuring points in order to obtain true displacements which were then used further on. Displacement correction is schematically shown in Fig. 8 and is conducted using following expression

$$\delta_{Li} = \delta_{LVDT,i} \text{ " } - \text{ " } \delta_{LVDT,10} \text{ " } - \text{ " } \frac{\delta_{LVDT,11}}{1740} l_i \quad \text{for } (i = 1,\ldots,4) \tag{6}$$

where δ_{Li} is displacement at measuring point Li after correction, $\delta_{LVDT,i}$, $\delta_{LVDT,10}$ and $\delta_{LVDT,11}$ are recorded values of displacement at measuring points Li, L10 and L11, respectively. l_i is the distance of the measuring point Li to the bottom edge of the specimen's base plate.

Next, specimen initial stiffness was calculated as the maximum value of secant stiffness obtained for the first three load steps for which the inelastic deformations of the specimens did not yet occur. This was done due to fact that initial stiffness of some specimens in subsequent load steps was greater than that in the first step. As the stiffness of the reaction frame alone was much higher compared to the test specimens, the inconsistency in the initial stiffness was considered as the consequence of additional small displacement of the reaction frame due to bolted connections between its elements, even though the bolts were pretensioned. Furthermore, the initial stiffness is prone to fabrication imperfections, and since the specimens were

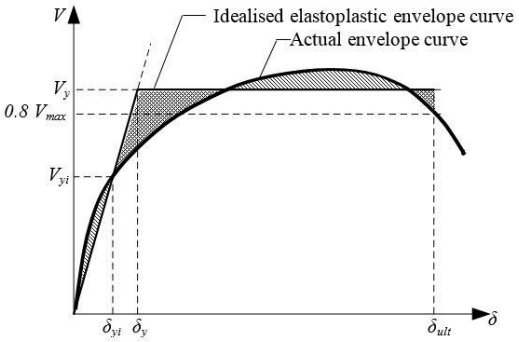

Fig. 9 Definition of the idealised elastoplastic envelope curve

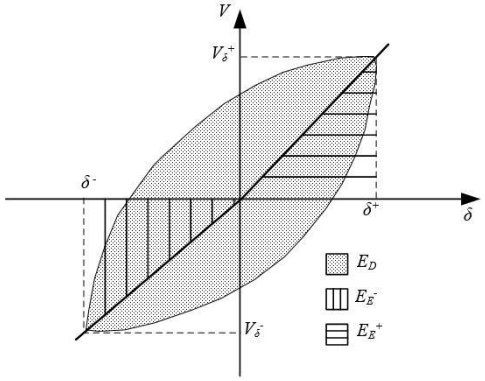

Fig. 10 Definition of energy dissipation capacity and equivalent viscous damping for one load cycle

scaled, small geometry variations could cause deviations of the initial stiffness.

Actual envelope curves of the test specimens were formed according to ATC (2010) connecting peak points of the first cycle of each load step. From the test results ultimate strength, corresponding to maximum force within the load piston, and ultimate displacement, δ_{ult}, were defined. The ultimate displacement, δ_{ult}, was defined in two ways depending on the shape of the actual envelope curve. If the actual envelope curve showed softening behaviour, δ_{ult} was defined as the value corresponding to 80% of the ultimate strength. However, for the envelope curves without softening behaviour δ_{ult} was set equal to the maximum displacement of the actual envelope that has been achieved during the test. Furthermore, to define characteristic values of the specimen behaviour, the initial yield point and the yield point, actual envelope curve had to be idealised with the elastoplastic envelope curve, Fig. 9. In order to define yield point (δ_y, V_y) concept of equal plastic energy had to be used so that the area enclosed by the idealised elastoplastic envelope curve equals to the area enclosed by actual envelope curve (Park *et al.* 2007). The point of the first inelastic behaviour (δ_{yi}, V_{yi}) was defined when the permanent residual deformation was developed due to cyclic loading for the first time.

Using previously obtained values global ductility of the system, μ_D, was determined as δ_{ult}/δ_y. Ability of the specimen to dissipate energy within one loading cycle equals to the area enclosed within the loop of the hysteretic curve, Fig. 10, and the total energy dissipation capacity of the specimen is summation of energy dissipated within each load cycle. Here, the mean values of specimen energy dissipation capacity per cycle of each load step will be calculated and compared. Since the number of load cycles, as well as storey displacement values, was not always exactly the same within specimen group during testing, energy dissipation capacity was not presented in cumulative manner, but as energy dissipation capacity for applicable storey displacement value. Additionally, another important indicator of cyclic behaviour is the value of specimen equivalent viscous damping, ζ_{eq}, which indicates energy absorption. Using definitions given in Fig. 10 equivalent viscous damping was calculated as

$$\zeta_{eq} = \frac{1}{2\pi}\frac{E_D}{E_E} = \frac{1}{2\pi}\frac{E_D}{(E_E^- + E_E^+)} = \frac{1}{2\pi}\frac{E_D}{\left(\frac{1}{2}V_\delta^-\delta^- + \frac{1}{2}V_\delta^+\delta^+\right)}, \quad (7)$$

where:

- E_D - dissipated energy within one load cycle of the load step (area enclosed by loop of hysteretic curve),
- E_E (E_{E-}, E_{E+}) - accompanying total elastic deformation energy (in negative and positive load direction),
- δ^-, δ^+ - highest value of displacement achieved within one load cycle of the load step (in negative and positive load direction),
- V_δ^-, V_δ^+ - corresponding force value for the highest displacement value achieved within one load cycle of the load step (in negative and positive load direction).

Finally, behaviour of the specimen under cyclic loading was observed through secant stiffness reduction in tension and compression. Average secant stiffness value, K_i^{sec}, for the *i*th load step was calculated as

$$K_i^{sec}\frac{\Sigma n V_i^n}{\Sigma n \delta_i^n} \ (\mathrm{i} = 1,2,\ldots,\mathrm{m}) \text{ and } (n = 2 \text{ or } 3), \quad (8)$$

where δ_i^n is the highest displacement in tension or compression of nth cycle of the *i*th load step, while V_i^n is the corresponding horizontal force at storey height.

Additionally, it is also important to mention that the load/displacement input was somewhat unsymmetrical, due to which the following experimental results are given separately for load cycle in compression (C) and tension (T). Also, most of the results are presented in comparison to storey drift ratio which has been calculated as the ratio of true storey displacement and storey height *H* (H = 1030 mm).

Experimental testing of the specimens was conducted up to the failure point or up to the point when its strength dropped to the value of about 80% of the ultimate strength obtained, either in tension or compression, during the test.

Table 4 Key results for specimen group F

Specimen	Initial stiffness [kN/mm]			Ultimate strength Force [kN]			Ultimate strength Displacement [mm]			Maximum displacement Force [kN]			Maximum displacement Displacement [mm]		
	(C)	(T)	mean	(C)	(T)	mean	(C)	(T)	mean	(C)	(T)	mean	(C)	(T)	mean
F100	13.6	13.8	13.7	207	209	208	68.1	69.2	68.7	160	157	159	81.6	79.0	80.3
F80	12.3	12.2	12.3	176	180	178	69.1	81.0	75.1	137	177	157	85.3	83.7	84.5
F60	10.5	10.8	10.7	139	135	137	61.9	41.7	51.8	134	105	120	65.0	64.3	64.7

Finally, it is important to note that, although the experimental test was conducted on specimens simulating bottom storey of SPSW the results as well as drawn conclusions are valid for any SPSW storey. This can be substantiated with the fact that columns at the bottom storey are usually fully fixed to the foundation (beam) due to stiff connection which is not the case with the columns at higher stories. Therefore, column flexural stiffness requirement at higher stories could probably be additionally reduced. Another important fact is also that greatest compression force occurs within the bottom storey columns, which again is more unfavourable condition regarding column flexural stiffness requirement than is the case for upper storey columns.

Fig. 11 Crack formation in HAZ at load step LS10 in specimen F80

4.2 Specimen group F - MRFs

Key experimental results of specimen group F regarding the initial stiffness, the achieved ultimate strength and the corresponding displacement, as well as the achieved maximum displacement and the corresponding force are given in Table 4.

As in Table 1. the obtained experimental results show that column flexural stiffness reduction results with decrease of specimen initial stiffness and ultimate strength. The calculated theoretical initial stiffness values are in good correlation with the experimentally obtained values where theoretical values of specimens F100, F80 and F60 are only by 10%, 6% and 0,5% higher than experimental ones, respectively. Furthermore, the obtained reductions of the initial stiffness and ultimate strength are slightly less than the reductions of the column flexural stiffness. Namely, the calculated initial stiffness mean value of specimen F80 is 90% (12.3 kN/mm/13.7 kN/mm), and of specimen F60 is 78% (10.7 kN/mm /13.7 kN/mm) of the mean value of initial stiffness of the reference specimen F100. Similarly, achieved ultimate strength mean value during testing of specimen F80 is 86% (178 kN/208 kN), and of specimen F60 is 66% (137 kN/208 kN) of the achieved ultimate strength mean value of the reference specimen F100.

In all of the MRF specimens first yielding occurred at point T1 positioned at the column bottom (Fig. 6) at approximately 1% story drift. Failure of all the specimens in specimen group F occurred in the heat affected zone (HAZ) of the column flange or the corresponding weld between outer column flange and base plate where a crack formed, Fig. 11. In the subsequent load cycles, after crack formation, the crack propagated into the column web after which the test was terminated. Crack formation within HAZ

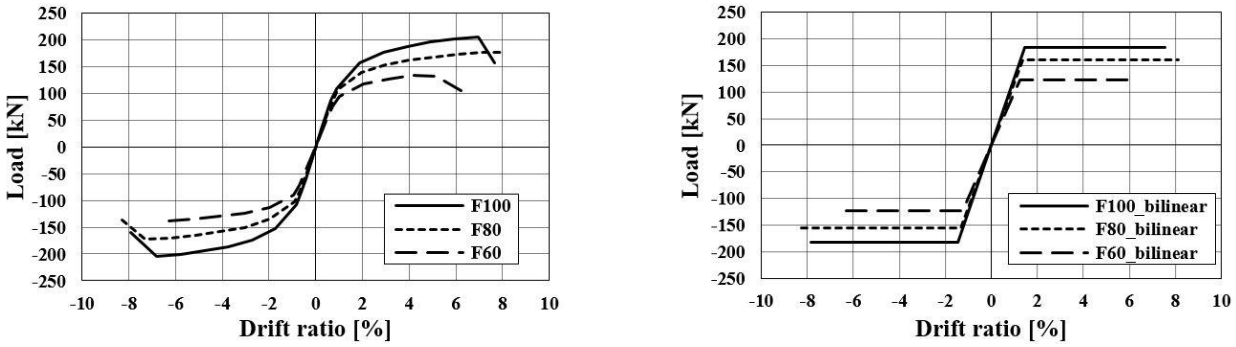

(a) Cyclic envelope curves

(b) Idealized bilinear envelope curves

Fig. 12 Specimen group F curves

Table 5 Parametehpgrs of idealized bilinear curves for specimen group F

Specimen	Initiation of inelastic behaviour				Yield point				Ultimate displacement		Ductility	
	V_{yi}	δ_{yi}	Direction	Critical location	V_y [kN]		δ_y [mm]		δ_{ult} [mm]		μ_D	
	[kN]	[mm]			(C)	(T)	(C)	(T)	(C)	(T)	(C)	(T)
F100	124	10.2	(C)	T1	183	184	15	15.1	80.6	77.7	5.4	5.1
F80	105	9.3	(T)	T1	155	161	13.7	14.2	85.0	83.7	6.2	5.9
F60	85	8.8	(C)	T1	124	123	12.9	12.8	64.8	64.0	5.0	5.0

for specimen F60 occurred in earlier load step than for other two specimens, which resulted in lower deformation capacity of specimen F60 which had least strength. However, specimen F60, despite that, showed stable behaviour of up to 4% drift ratio.

Fig. 12(a) shows cyclic envelope curves of each F specimen while specimen cyclic curves are shown in Fig. 21. Idealisation of the actual envelope curves resulted in bilinear envelope curves, Fig 12(b), whose parameters are given in Table 5. Curve idealisation is based on strain gauge records for which first inelastic behaviour occurs, i.e., strain gauge at critical location which for all F specimens was at the measuring place T1, where column flange deformations were recorded.

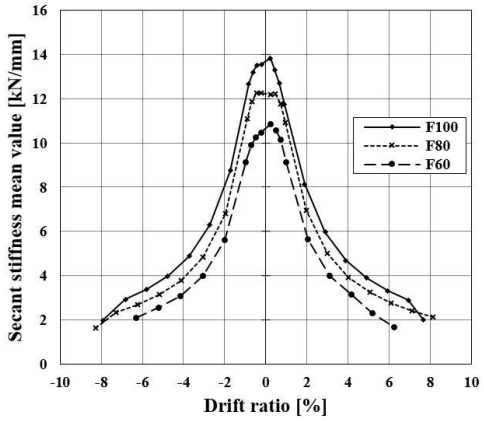

Fig. 13 Specimen group F secant stiffness reduction

Fig. 13 presents reduction of secant stiffness during testing. For all F specimens initial stiffness values as well as secant stiffness values, during the entire test, display clearly visible difference. It is also important to note stable secant stiffness reduction for all specimens indicating that column flexural stiffness reduction does not have negative impact on the behaviour of MRFs under cyclic loading, as is expected. Energy dissipation capacity as well as equivalent viscous damping coefficient values per load cycle of each load step were calculated and presented in section 4.4.

In order to obtain profiles of column horizontal displacements during laboratory testing vertical displacements were measured along the frame column at the measuring points L1 to L4 (Fig. 6). The resulting column profiles for the specimen group F at the drift ratios of approximately 2% and 4% are shown in Fig. 14(a)-(b), respectively. The obtained results confirm the fact that flexural stiffness of columns which are part of MRFs does not have impact on the resulting horizontal displacement profiles, what is expected since there are no additional transverse forces acting on columns as the consequence of tension field action.

4.3 Specimen group S - SPSWs

Key experimental results of specimen group S regarding the initial stiffness, the achieved ultimate strength and the corresponding displacement, as well as the achieved maximum displacement and the corresponding force are given in Table 6.

As in Table 1. the results show that change in column

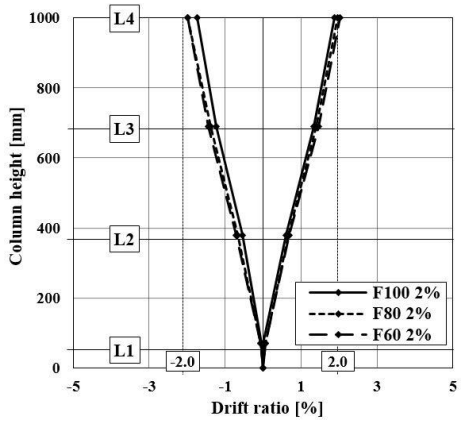

(a) 2% drift

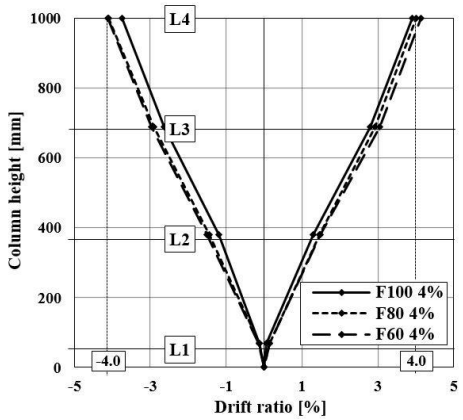

(b) 4% drift

Fig. 14 Column horizontal displacement profiles for specimen group F

Table 6 Key results for specimen group S

Specimen	Initial stiffness [kN/mm]			Ultimate strength Force [kN]			Ultimate strength Displacement [mm]		Maximum displacement Force [kN]			Maximum displacement [kN/mm]		
	(C)	(T)	mean		(C)	(T)	mean		(C)	(T)	mean		(C)	(T)	mean
S100	94	106	100	**S100**	94	106	100	**S100**	94	106	100	**S100**	94	106	100
S80	73	76	75	**S80**	73	76	75	**S80**	73	76	75	**S80**	73	76	75
S60	95	83	89	**S60**	95	83	89	**S60**	95	83	89	**S60**	95	83	89

(a) Infill panel corner

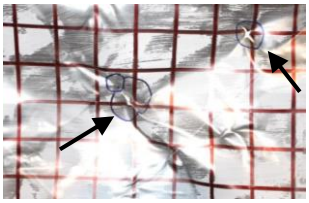

(b) Within infill plate at points of "kinks"

(c) At HAZ and propagation into column web at load step LS20b (specimen S60)

Fig. 15 Specimen group S cracks

flexural stiffness has negligible impact on the initial stiffness value of S specimens, where the initial stiffness is almost one order of magnitude higher than the initial stiffness obtained for the F specimens. The calculated theoretical initial stiffness values are in good correlation with the experimentally obtained values except for specimen S80. Mean values of experimentally obtained initial stiffness of specimens S100, S80 and S60 deviate from theoretical values which are by 3%, 26% and 7% higher than experimental ones, respectively. Although initial imperfections of the specimens have not been measured, high deviation of initial stiffness that has occurred for specimen S80 is attributed to the initial imperfections and residual stresses inside the specimen as a consequence of welding process. As it is obvious that steel plate significantly increases initial stiffness when added to MRF, it is therefore concluded that the steel infill plate imperfections were most probably responsible for such great deviation of initial stiffness within the specimen S80. Also, since the test specimens were scaled, fabrication errors could additionally have higher impact on the initial stiffness value, than it would be the case with fully scaled specimens.

Reduction of column flexural stiffness resulted in decrease of specimen ultimate strength. Namely, the achieved ultimate strength mean value of specimen S80 is 92% (342 kN/371 kN), while of specimen S60 is 87% (321 kN/371 kN) of the ultimate strength mean value achieved by the reference specimen S100. As expected, since the infill plate contributes to the strength of SPSWs, reduction of the ultimate strength, in percentage, is smaller compared to the strength reduction obtained for F specimens.

First cracks in S specimens develop at the infill plate corners, i.e., at the weld between two adjacent fish plates in the corners close to the specimens beam, Fig. 15(a). These cracks in later steps propagate to the centre of infill plate. With the progress of the test as the tension diagonals, due to load direction change, intersect cracks start to open at the points where multiple panel folding of the plate occurs, at so called panel "kinks", Fig. 15(b). Although numerous cracks within the plate have been formed, ultimate strength of the specimen still has not been reached. Ultimate strength of all S specimens was reached when the crack formed in the HAZ at column bottom at the connection of the column outside flange and base plate. In the subsequent load cycles the crack propagated to the column web after which the test was terminated, Fig. 15(c). Fig. 16 shows specimen S100

Fig. 16 Specimen S100 after testing

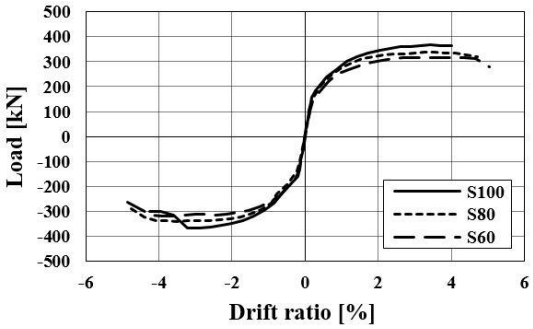

(a) Cyclic envelope curves

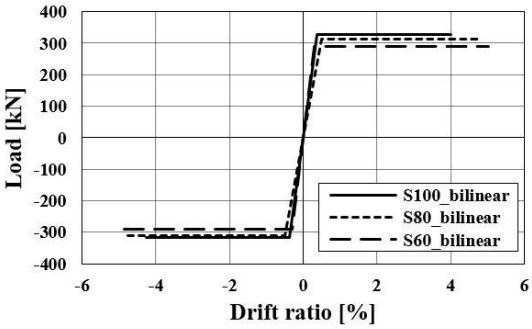

(b) Idealized bilinear envelope curves

Fig. 17 Specimen group S curves

Table 7 Phparameters of idealized bilinear curves for specimen group S

Specimen	Initiation of inelastic behaviour				Yield point				Ultimate displacement		Ductility	
	V_{yi}	δ_{yi}	Direction	Critical location	V_y [kN]		δ_y [mm]		δ_{ult} [mm]		μ_D	
	[kN]	[mm]			(C)	(T)	(C)	(T)	(C)	(T)	(C)	(T)
F100	117	1.4	(C)	Ro3	316	328	3.8	3.9	43.9	41.3	11.6	10.6
F80	129	2.1	(C)	Ro3	311	313	5.1	5.1	48.9	48.6	9.6	9.6
F60	105	1.1	(C)	Ro3	290	289	3.0	3.0	50.1	51.9	16.7	17.3

after testing, where characteristic X-shaped out-of-plane displacement of the infill plate, due to tension diagonal (tension field) formation, can be seen.

Cyclic envelope curves of S specimens are given in Fig. 17(a), while specimen cyclic curves are shown in Fig. 21. Idealisation of the actual envelope curves resulted in bilinear envelope curves, Fig. 17(b), whose parameters are given in Table 7. Curve idealisation is based on strain gauge records for which first inelastic behaviour occurs, i.e., strain gauge at critical location which for all S specimens was at the infill plate (gauges R7, R8 and R9), i.e., at the measuring place Ro3. As expected the idealized results obtained for S80 differ somewhat form the other results which is the consequence of lower initial stiffness value that has impact on the parameters of idealized elastoplastic curves.

Secant stiffness values calculated according to Eq. (8) exhibit stable reduction throughout the entire test for all S specimens, Fig. 18. Variation of initial stiffness between specimens, previously explained, did not have negative impact on the overall specimen behaviour. Finally, these results confirm stable and acceptable behaviour of all S specimens up to 4% storey drift ratios, even though their columns did not satisfy prescribed condition regarding minimal flexural stiffness. Energy dissipation capacity as well as equivalent viscous damping coefficient values per load cycle of each load step are presented in section 4.4.

Horizontal displacement profiles of columns within specimen group S are shown in Fig. 19. The results for two storey drift ratios, 2.5% and 4%, were obtained and are shown in Figs. 19(a)-(b), respectively. Since different yield displacement values are used for each specimen group drift ratios used here are somewhat different from the drift ratios

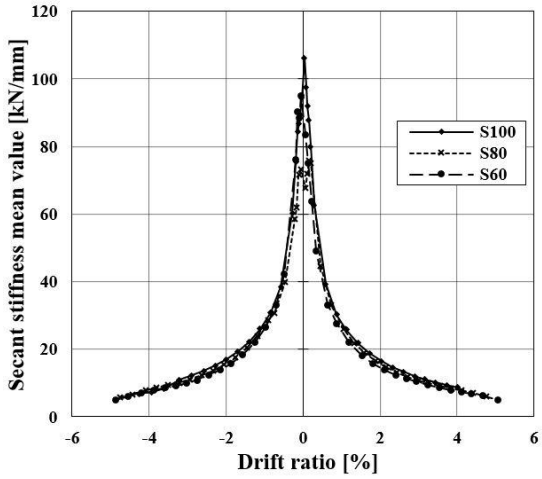

Fig. 18 Specimen group S secant stiffness reduction

used with F specimens. Contrary to the results of F specimens, S specimens show "pull-in" behaviour of their columns because of the transverse loads which are consequence of the tension field action within the infill steel plate. The "pull-in" behaviour of the columns is recorded at the measuring place L1 where the transverse action from the infill panel is most pronounced. Also, the amount of column "pull-in", as is expected, increases with the reduction of column flexural stiffness. Even though column of specimen S60 showed the largest amount of "pull-in", the measured amount is still insignificant and did not have negative impact on the overall specimen behaviour, i.e., did not cause sudden reduction of secant stiffness for drift ratios of up to 4%, Fig. 19.

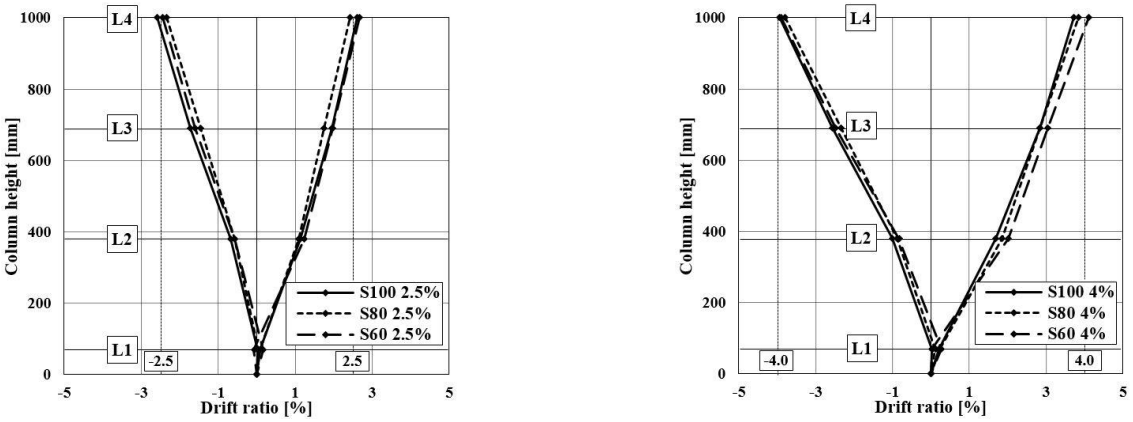

(a) 2.5% drift (b) 4% drift

Fig. 19 Column horizontal displacement profiles for specimen group S

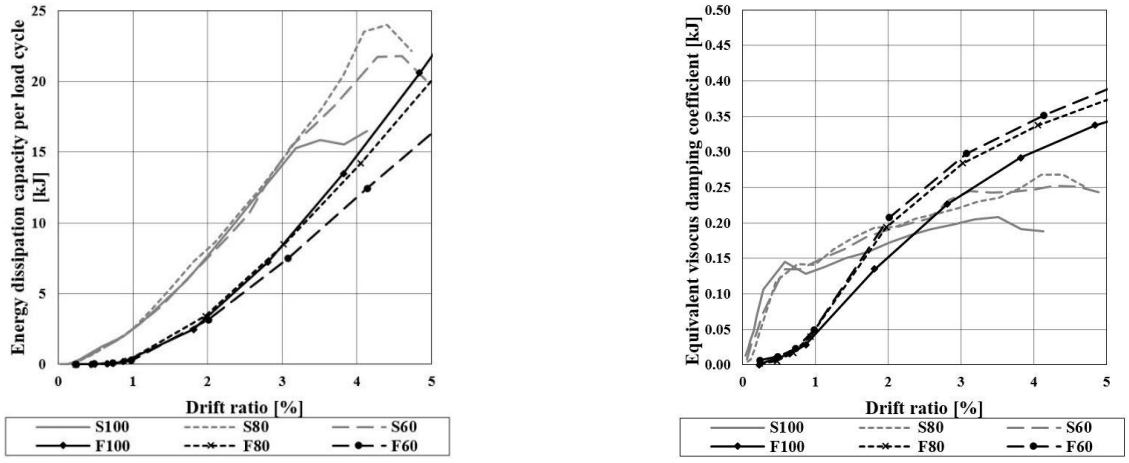

(a) Energy dissipation capacity (b) Equivalent viscous damping coefficient

Fig. 20 Comparison of specimens results

4.4 Results comparison

Even though the tests were conducted on small-scale specimens the obtained results offer reliable basis to retrieve valid conclusions regarding influence of column flexural stiffness on the overall MRF and SPSW systems behaviour.

As expected, the obtained results show that steel plate placed within the MRF increases initial stiffness of the specimen. The increase was almost ten times, due to which the change of column flexural stiffness had almost negligible influence on the initial stiffness of S specimens. Furthermore, the change of column flexural stiffness also impacts specimen's ultimate strength where the change is more pronounced for F specimens. Namely, highest column flexural stiffness reduction of 36% causes ultimate strength reduction of 34% (137 kN/208 kN), Table 4, and only 13% (321 kN/371 kN), Table 6, for specimen group F and S, respectively. Additionally, mean value of the difference between ultimate strengths of corresponding S and F specimens was calculated and amounts to 170 kN. This correlates well with the mean value of the infill panel shear strength which is 172 kN, and was calculated using Eq. (1) and experimentally obtained steel material ultimate strength value from Table 3. Therefore, this obviously indicates equal utilization of the infill plate for all specimens, i.e., that the tension field was able to develop in all of S specimens regardless of the column flexural stiffness.

Energy dissipation capacity as well as equivalent viscous damping coefficient values per load cycle of each load step for all the specimens were calculated and compared in Figs. 20(a)-(b), respectively. For specimen group F, as expected, higher column flexural stiffness enables higher values of energy dissipation capacity while at the same time slightly higher values of viscous damping coefficient are obtained for "weaker" specimens. On the other hand specimens within specimen group S show almost no difference between dissipation capacity values up to a drift ratio of 3% specimens, while for equivalent viscous damping values difference is negligible for drift ratios up to 0.7%. Again, "weaker" S specimen exhibit slightly higher values of equivalent viscous damping after 0.7% drift ratio.

Experimentally obtained hysteretic curves with corresponding envelope curves of both specimen groups are shown in Fig. 21. Comparing the two specimen groups one can see that for F specimens force-deformation loops are

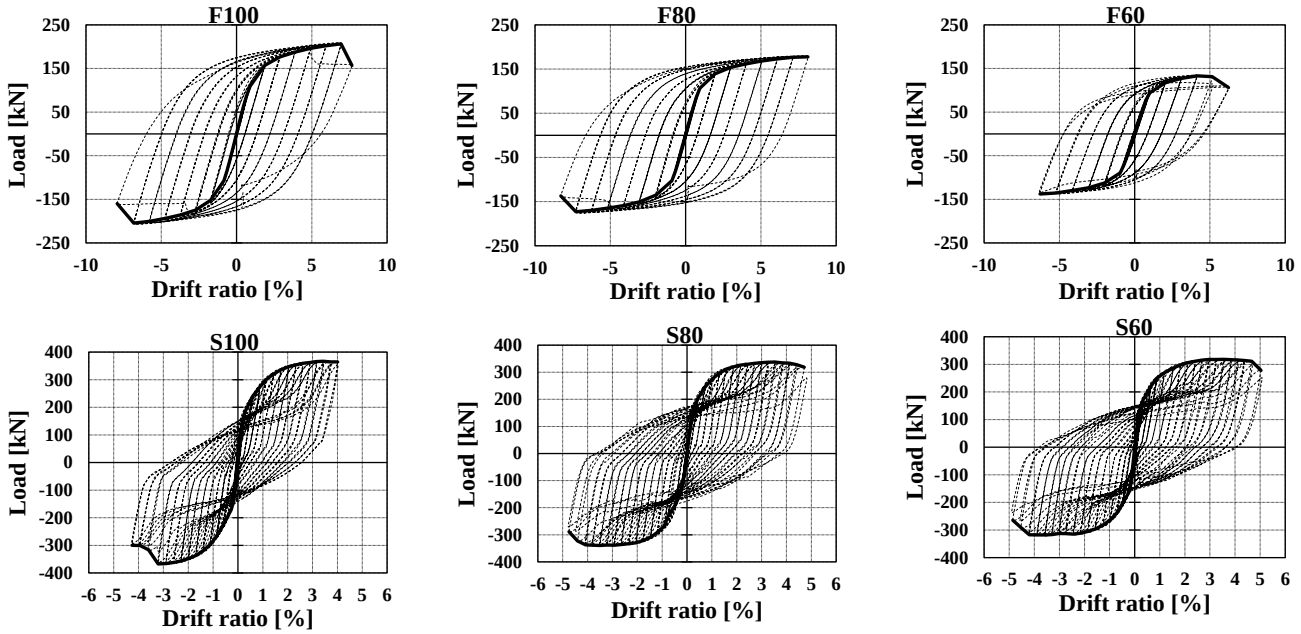

Fig. 21 Experimental hysteretic curves with corresponding envelope curves

wide and open while the ones of S specimens are somewhat pinched in the middle. Pinched curves usually characterize less ductile structures that are unable to dissipate large amounts of energy, (FEMA 2009), but such direct comparison between different vertical stabilization systems, here MRFs and SPSWs, is not possible. Therefore, valid comparison of the two different vertical stabilization systems is given in Fig. 20. The energy dissipation capacity of S specimens up to their failure point, even though they show pinched hysteretic curves, is greater than the energy dissipation capacity of F specimens. On the other hand the value of equivalent viscous damping coefficient of S specimens is higher than of F specimens only up to a storey drift ratio of approximately 2%, indicating that ultimate resistance of SPSWs is, at that point, almost reached.

5. Development and validation of finite element model

5.1 General

Finite element models of the tested specimens were developed before the experiments were conducted using commercially available finite element software Ansys 14.5, (ANSYS 2012). In that step FE models were used to obtain yield displacement, δ_y, needed for formation of loading protocol of MRF and SPSW specimens. After the experimental investigation, the models were calibrated according to results and observations noted during experimental testing. Calibration of FE models was necessary in order to obtain reliable models needed for further parametric numerical analyses.

5.2 Modelling assumptions

Three dimensional models using static structural analysis module in Workbench, which uses implicit solving methods, were created in Ansys 14.5, (ANSYS 2012). Due to complexity of achieving numerical convergence 4-node shell elements SHELL181 were chosen for all simulated elements (frame elements and the infill plates). Such models were able to account for the complex stress distribution that is present in the infill panel as well as in the columns and beams and, in addition, allow simulation of initial imperfections of the steel infill panel. Connections between infill plate and the boundary frame elements as well as beam-to-column connections were simulated as coupled connections in order to reduce the complexity of the model.

In order to further reduce FE model complexity, reaction frame, out-of-plane support, base plate as well as rigid adapter for the force/displacement input were not explicitly modelled. Connection of the columns and bottom fish plate to the base plate, and then to the reaction frame were simulated using fixed supports preventing all six degrees of freedom. The simulation of out-of-plane support was such that it only prevented displacement in global Z direction. Displacement input was conducted over number of edges in order to simulate rigid adapter used during the experiment. Finite element models were tested under monotonic loading, i.e., pushover analyses for both load directions were conducted. Aforementioned simulations of various boundary conditions are presented in Fig. 22(a). In addition, initial imperfection was also taken into account when defining FE models. The shape of the imperfection corresponded to the first buckling mode shape of the plate under pure shear loading, Fig. 22(b). The magnitude of the initial imperfection was equal to $\sqrt{LH}/1000$, since further increase of its value did not have significant impact on the model initial stiffness and overall behaviour. Simulation of initial imperfection was necessary in order to simulate perfect geometry to buckle and form the tension diagonal.

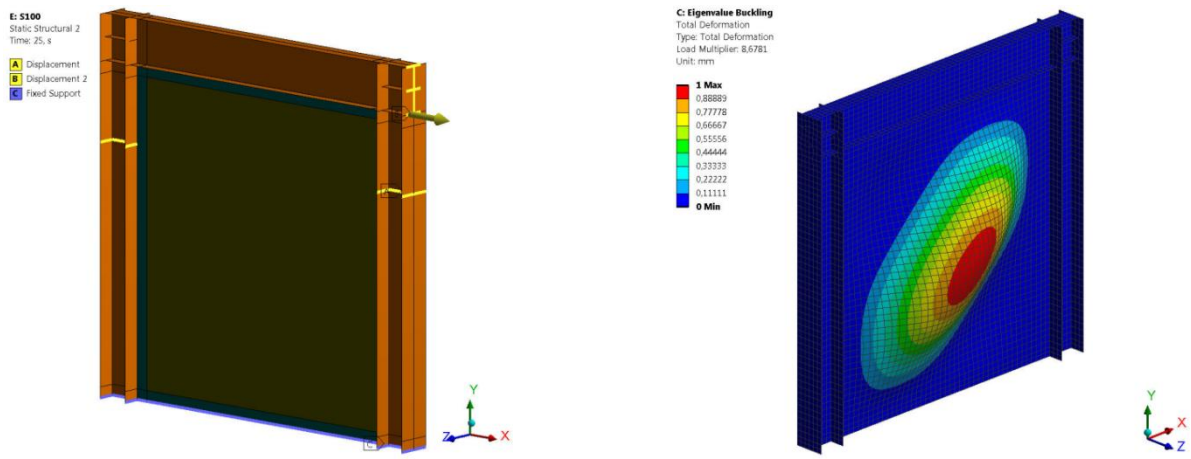

(a) Boundary conditions

(b) First buckling mode shape of plate with clamped boundary conditions loaded in pure shear

Fig. 22 Finite element simulations

Even though the mesh size could be bigger, the selected size used in our FE models is between 15 and 20 mm.

5.3 Material models

Properties of the steel material have been determined using standard tensile test of the steel probes, and the obtained results are given in Table 3. Since steel material under monotonic and cyclic load behaves differently, Fig. 23, application of the obtained material values for FE simulation of cyclically tested specimens can lead to incorrect results. Therefore, the material stress-strain curves used in FE simulations were determined using approach proposed by Budahazy (2015), where using three material parameters determined from monotonic tensile test one can derive stress-strain curve of the material under cyclic load. However, this approach was applied for all used steel materials except for the steel material of the infill panel. Infill panel presents very slender element which can only carry negligible amount of compression force. Therefore, in reality, steel material of the infill plate will only be loaded in tension which approves use of stress-strain curves obtained from standard tensile testing. Additionally, the proposed approach was slightly modified in the part that it does not take into account isotropic, but only kinematic hardening of the material. Failure of the material has not been simulated. More details on material modelling can be found in (Curkovic 2017).

5.4 Results and FE model validation

The obtained FE pushover curves for each loading direction were compared to the hysteretic force-displacement curves recorded during the experimental investigation. Since failure of the test specimens occurred due to crack formation at the column bottom and material failure has not been taken into account it is obvious that such failure mechanism cannot be properly simulated. But simulations are expected to correlate well up to the point of crack opening which in the experimental testing never occurred before 2.5% storey drift ratio which is assumed to be the ultimate displacement limit according to EN 1998-1 (CEN 2004).

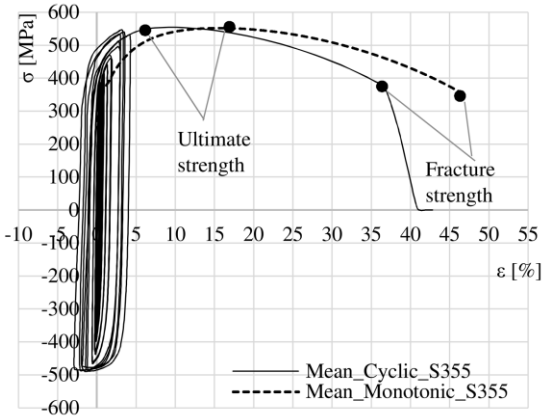

Fig. 23 Stress-strain curves of steel S355 obtained under monotonic and cyclic testing, (Krolo *et al.* 2016)

The comparison of FE pushover curves in tension and compression with experimentally obtained hysteretic curves for specimen group F and S are shown in Fig. 24. Graphically results seem to compare well, but for more detailed analysis results are compared regarding initial stiffness values as well as realized strength for corresponding storey drift ratios. For that purpose percentage of error of numerical to experimental value was calculated using following expression

$$ERR. = \frac{FEM. - EXP.}{EXP.} \tag{9}$$

where *FEM.* indicates mean value for results of numerical analysis, while *EXP.* indicates mean value obtained for results of experimental analysis. Percentage of error can have negative or positive value if numerically obtained result is lower or higher than experimentally obtained result, respectively.

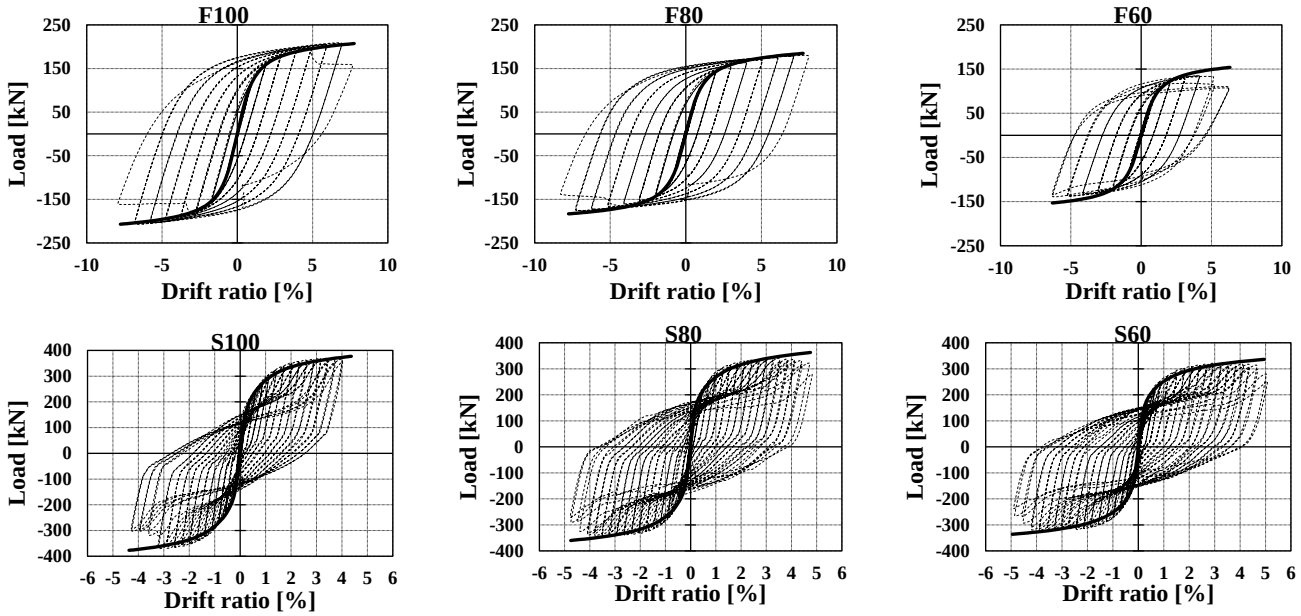

Fig. 24 Comparison of experimental hysteretic curves with corresponding FE pushover curves

Experimental and numerical results of all tested specimens are given in Table 8. The amount of realized horizontal load is, for F specimens, compared for two storey drift ratios, namely ±2.5% and 4%. The highest strength deviations of 7.0% and 5.3% were obtained for specimen F60 at ±2.5% storey drift ratio, and specimen F80 at ±4% storey drift ratio, respectively. On the other hand, amount of realized horizontal force for drift ratio of ±2.5% for numerical SPSW models was always lower than for tested specimens, where largest deviation of -3.3% was obtained for specimen S100.

Comparison of numerical and experimental initial stiffness values shows good correlation where numerically obtained values are somewhat greater than the experimental ones. High deviation is only noticed for specimen S80, whose numerical value is 42.3% higher than the experimental results. This can, obviously, be contributed to significant initial imperfections within specimen S80 due to which experimental value of initial stiffness was also inconsistent with theoretically obtained value given in Table 1. Furthermore, comparing initial stiffness values it can be seen that numerically obtained ones for MRF show smaller while for SPSW show higher values than theoretically obtained values. Therefore, for specimens F100, F80 and F60 variation of initial stiffness is about -6%, -2% and -1%, respectively, while for specimens S100, S80 and S60 is 2%, 6% and 6%, respectively.

Finally, the column displacement profiles obtained experimentally and numerically could not be compared since VBE "pull-in" deformation can only occur if the specimens are cyclically loaded. For that purpose, numerical finite elements simulations including cyclic loading of the specimens need to be developed.

6. Conclusions

Within this paper experimental and numerical studies of MRF and SPSW specimen with variable column second area moment values were conducted in order to investigate the impact of column flexural stiffness on the seismic performance of the SPSW systems. For that purpose, three one-storey one-bay MRF and SPSW specimens were designed, fabricated and tested. In order to fulfil strength requirements boundary elements were designed using capacity design approach. Specimens within each specimen group were identical except for column flexural stiffness which was varied through the reduction of column flanges width. Finite element models of the specimens were developed for two stages. For the first stage they were developed in order to define the yield point necessary for definition of loading protocol using experimentally obtained steel material data. For the second stage finite element models were modified based on experimental results and observations. Based on the obtained results following can be concluded:

- initial stiffness of SPSWs is mostly influenced by the infill panel. This is especially pronounced for SPSWs with low column flexural stiffness values, where initial stiffness of SPSW compared to corresponding MRF was almost ten times higher;
- theoretically obtained values of initial stiffness show good correlation with the experimental values, except for specimen S80 probably as a consequence of fabrication errors and initial imperfections that exist within the infill plate;
- column flexural stiffness reduction of 36% did not impact SPSW system cyclic ductility where all of the specimens tolerated story drift ratios of more than 4%;

- all SPSW specimens showed stable secant stiffness reduction throughout the entire test even though the minimum flexural stiffness values of VBEs were not satisfied;
- insignificant "pull-in" deformation of VBEs near their base connection was observed even for storey drift ratios of 4%;
- "pull-in" of the VBEs did not have negative impact on the overall SPSW system behaviour which is clearly visible from stable secant stiffness reduction, as well as energy dissipation and damping capacity diagrams;
- the steel infill panel was completely utilized regardless of the applied column flexural stiffness which has also been even analytically confirmed;
- developed FE models with adopted constitutive model to take into account cyclic behaviour of material can reasonably well predict global behaviour of SPSWs using pushover analysis. Therefore, such FE models can further be used for purpose of numerical parametric analyses. Additionally, use of shell elements proved to be valid as their application drastically reduced computational time and provided reliable results.

Finally, from the above conclusions, this research has indicated that current requirement for column flexural stiffness used for SPSWs might be conservative and needs to be further investigated using either experimental or numerical research methods.

Acknowledgments

The authors thank prof. J.F. Hajjar at Northeastern University for his contribution through many advices within this specific research field.

References

AISC (2010), ANSI/AISC 341-10: Seismic Provisions for Structural Steel Buildings; American Institute of Steel Construction (AISC), Chicago, IL, USA.

ANSYS (2012), User's Manual (Version 14.5); Swanson Analysis Systems Inc., Houston, TX, USA.

Astaneh-Asl, A. (2001), "Seismic Behavior and Design of Steel Shear Walls", Steel TIPS Report; Structural Steel Education Council, Moraga, CA, USA.

ATC (1992), ATC-24: Guidelines for Cyclic Seismic Testing of Components of Steel Structures; Applied Technology Council, Redwood City, CA, USA.

ATC (2010), PEER/ATC-72-1: Modelling and Acceptance Criteria for Seismic Design and Analysis of Tall Buildings; Applied Technology Council, Redwood City, CA, USA.

Basler, K. (1961), "Strength of Plate Girders in Shear, Proc. ASCE, 87, (ST7), (October 1961), Reprint No. 186 (61-13)", Fritz Laboratory Reports; Paper 70.

Berman, J.W. and Bruneau, M. (2003), "Plastic analysis and design of steel plate shear walls", *J. Struct. Eng.*, **126**(11), 1448-1456. https://doi.org/10.1061/(ASCE)0733-9445(2003)129:11(1448)

Budahazy, V. (2015), "Uniaxial cyclic steel behavior and model for dissipative structures", Ph.D. Dissertation; Budapest University of Technology and Economics, Budapest, Hungary.

CEN (2004), EN 1998-1: Eurocode 8. Design of structures for earthquake resistance – Part 1: General rules, seismic actions and rules for buildings; European Committee for Standardization, Brussels, Belgium.

CEN (2005), EN 1993-1-1: Eurocode 3: Design of steel structures – Part 1-1: General rules and rules for buildings; European Committee for Standardization, Brussels, Belgium.

CEN (2009), EN ISO 6892-1:2009 – Metallic materials – Tensile testing – Part 1: Method of test at room temperature; European Committee for Standardization, Brussels, Belgium.

CSA (2009), S16-09 Design of Steel Structures; Canadian Standards Association, Toronto, ON, Canada.

Curkovic, I. (2017), "Behaviour of composite plate shear walls under earthquake", Ph.D. Dissertation; University of Zagreb, Zagreb, [in Croatian].

Curkovic, I. and Dzeba, I. (2016), "State of the art review on behaviour and calculation of composite plate shear walls", *Tehnicki Vjesnik-Technical Gazette*, **23**(5) 1523-1532. https://doi.org/10.17559/TV-20141111103014

Curkovic, I., Skejic, D. and Dzeba, I. (2017), "11.24: Impact of column flexural stiffness on behaviour of steel plate shear walls", *ce/papers*, **1**(2-3), 3023-3032. https://doi.org/10.1002/cepa.354

Driver, R.G., Kulak, G.L., Kennedy, J.L. and Elwi, A.E. (1998), "Cyclic test of four-story steel plate shear wall", *J. Struct. Eng.*, **124**(2), 112-120. https://doi.org/10.1061/(ASCE)0733-9445(1998)124:2(112)

ECCS (1985), Recommended Testing Procedures for Assessing the Behavior of Structural Elements Under Cyclic Loads; European Convention for Constructional Steelwork, Technical Committee 1, TWG 1.3 – Seismic Design, No. 45, Brussels, Belgium.

Elgaaly, M., Caccese, V. and Du, C. (1993), "Postbuckling behavior of steel plate shear walls under cyclic loads", *J. Struct. Eng.*, **119**(2), 588-605. https://doi.org/10.1061/(ASCE)0733-9445(1993)119:2(588)

FEMA (2009), FEMA P-750: NEHRP Recommended Seismic Provisions for New Buildings and Other Structures; Building Seismic Safety Council, Washington, D.C., USA.

Kalali, H., Hajsadeghi, M., Zirakian, T. and Alaee, F.J. (2015), "Hysteretic performance of SPSWs with trapezoidally horizontal corrugated web-plates", *Steel Compos. Struct., Int. J.*, **19**(2), 277-292. https://doi.org/10.12989/scs.2015.19.2.277

Krolo, P., Grandic, D. and Smolcic, Z. (2016), "Experimental and numerical study of mild steel behaviour under cyclic loading with variable strain ranges", *Adv. Mater. Sci. Eng.* http://dx.doi.org/10.1155/2016/7863010

Kuhn, P., Peterson, J.P. and Levin, L.R. (1952), A Summary of Diagonal Tension Part I: Methods and Analysis, Technical Note 2661; National Advisory Committee for Aeronautics, Washington, D.C., USA.

Lubell, A.S., Prion, H.G.L., Ventura, C.E. and Rezai, M. (2000), "Unstiffened steel plate shear wall performance under cyclic loading", *J. Struct. Eng.*, **126**(4), 453-460. https://doi.org/10.1061/(ASCE)0733-9445(2000)126:4(453)

Machaly, E.B., Safar, S.S. and Amer, M.A. (2014), "Numerical investigation on ultimate shear strength of steel plate shear walls", *Thin-Wall. Struct.*, **84**, 78-90. https://doi.org/10.1016/j.tws.2014.05.013

Montgomery, C.J. and Medhekar, M. (2001), "Unstiffened steel plate shear wall performance under cyclic loading", *J. Struct. Eng.*, **127**(8), 973-975. https://doi.org/10.1061/(ASCE)0733-9445(2001)127:8(973)

Park, H.G., Kwack, J.H., Jeon, S.W., Kim, W.K. and Choi, I.R. (2007), "Framed steel plate wall behavior under cyclic lateral

loading", *J. Struct. Eng.*, **133**(3), 378-388. https://doi.org/10.1061/(ASCE)0733-9445(2007)133:3(378)
Purba, R. and Bruneau, M. (2010), Impact of Horizontal Boundary Elements Design on Seismic Behavior of Steel Plate Shear Walls, Technical Report MCEER-10-0007; Multidisciplinary Center for Earthquake Engineering Research, University of New York at Buffalo, Buffalo, NY, USA.
Purba, R. and Bruneau, M. (2014), Seismic Performance of Steel Plate Shear Walls Considering Various Design Approaches. Technical Report MCEER-14-0005; Multidisciplinary Center for Earthquake Engineering Research, University at Buffalo, State University of New York, Buffalo, NY, USA.
Qu, B. and Bruneau, M. (2010), "Behaviour of vertical boundary elements in steel plate shear walls", *Eng. J.*, **47**, 109-122.
Qin, Y., Lu, J., Huang, L.C.X. and Cao, S. (2017a), "Flexural behavior of beams in steel plate shear walls", *Steel Compos. Struct., Int. J.*, **23**(4), 473-481. https://doi.org/10.12989/scs.2017.23.4.473
Qin, Y., Lu, J.Y., Huang, L.C.X. and Cao, S. (2017b), "Flexural ehavior of anchor horizontal boundary element in steel plate shear wall", *Int. J. Steel Struct.*, **17**(3), 1073-1086. https://doi.org/10.1007/s13296-017-9017-6
Rahmzadeh, A., Ghassemieh, M., Park, Y. and Abolmaali, A. (2016), "Effect of stiffeners on steel plate shear wall systems", *Steel Compos. Struct., Int. J.*, **20**(3), 545-569. https://doi.org/10.12989/scs.2016.20.3.545
Sabelli, R. and Bruneau, M. (2007), Steel Design Guide 20 – Steel Plate Shear Walls; American Institute of Steel Construction (AISC), USA.
Sabouri-Ghomi, S. and Sajjadi, S.R.A. (2012), "Experimental and theoretical studies of steel shear walls with and without stiffeners", *J. Constr. Steel Res.*, **75**, 152-159. https://doi.org/10.1016/j.jcsr.2012.03.018
Thorburn, G.L., Kulak, L.J. and Montgomery, C.J. (1983), Analysis of Steel Plate Shear Walls, Structural Engineering Report No. 107; University of Alberta, Edmonton, Alberta, Canada.
Timoshenko, S. and Young, D.H. (1968), *Elements of Strength of Materials*, (5th Edition), Van Nostrand, Princeton, NJ, USA.
Tsai, K.C., Li, C.H. and Lee, H.C. (2014), "Seismic design and testing of the bottom vertical boundary elements in steel plate shear walls. Part 1: design methodology", *Earthq. Eng. Struct. Dyn.*, **43**, 2237-2259. https://doi.org/10.1002/eqe.2443
Vian, D. (2005), "Steel plate shear walls for seismic design and retrofit of building structures", Ph.D. Dissertation; University of New York at Buffalo, Buffalo, NY, USA.
Wagner, H. (1931), Flat Sheet Metal Girders with Very Thin Webs, Part III: Sheet Metal Girders with Spars Resistant to Bending – The Stress in Uprights – Diagonal Tension Fields, Technical Memorandum No. 606; National Advisory Committee for Aeronautics, Washington, D.C., USA.

CC